Journal of Fluids and Structures 17 (2003) 701–715

JOURNAL OF FLUIDS AND STRUCTURES

www.elsevier.nl/locate/jnlabr/yjfls

Low-frequency fluctuations in the near-wake region of a trapezoidal cylinder with low aspect ratio

J.J. Miau[a,*], J.T. Wang[a], J.H. Chou[b], C.Y. Wei[c]

[a] *Institute of Aeronautics and Astronautics, Department of Aeronautics and Astronautics, National Cheng Kung University, Tainan 70101, Taiwan, ROC*

[b] *Department of Engineering Science, National Cheng Kung University, Tainan, Taiwan 701, ROC*

[c] *Department of Aeronautics, Air Force Academy, Taiwan, ROC*

Received 28 February 2001; accepted 15 November 2002

Abstract

Base pressure signals obtained on a trapezoidal cylinder with an aspect ratio 4.7, at Reynolds numbers of the order of 10^4, were examined after being low-pass filtered at different cut-off frequencies. For the range of the Reynolds numbers studied, the integral time scales of the low-passed fluctuations versus the cut-off frequencies chosen was found to fall on a curve. Cross-correlation between the pressure fluctuations measured at the cylinder base and the velocity fluctuations detected in the near-wake region were examined with the signal traces low-passed at different cut-off frequencies. Accordingly, an optimal cut-off frequency was defined as the one corresponding to the highest correlation obtained. The integral time scale of the low-passed fluctuations in reference to the optimal cut-off frequency was found to be about two times the vortex-shedding period. The low-frequency variations measured appeared to be insensitive to the artificial tripping to the sidewall boundary layer, and exhibited a global behavior in a near-wake region.
© 2003 Elsevier Science Ltd. All rights reserved.

1. Introduction

The presence of low-frequency fluctuations in vortex shedding behind a bluff body has attracted researchers' attention for decades. Some earliest works in this respect are briefly described below. Roshko (1954) made hot-wire measurements in the wake of a circular cylinder and noticed that in the range of Reynolds numbers between 150 and 300 irregular bursting signals appeared in the oscillogram obtained. Roshko (1954) addressed that this phenomenon was the cause leading to scattering in the measurement of shedding frequency. The oscillogram showed that the characteristic period of irregular bursts was of about 10 times the shedding period. From the dye visualization and velocity measurements made at several points in the wake behind a circular cylinder, Tritton (1959) observed two modes of Karman vortex shedding, one of which was a low-speed mode in the range of $40 < \mathrm{Re} < 110$ and the other was a high-speed mode in the range of $80 < \mathrm{Re} < 160$. The low- and high-speed modes differed in their shedding frequencies, and the transition between them was characterized by periodic beating, which was of the order of 6–14 times the primary shedding period. Bloor (1964) noted the presence of low-frequency unsteadiness in the velocity signals measured in the near-wake region behind a circular cylinder for Reynolds numbers ranging from 300 to 500. Bloor (1964) further suggested that the low-frequency variations are associated with the development of three dimensionality of vortex-shedding structures. In studying the three-dimensional structure of the wake behind a circular cylinder, Gerrard (1966a) noticed that the amplitude of low-frequency fluctuations in a velocity signal trace measured could be correlated with the

*Corresponding author. Tel.: +886-6-275-7575; fax: +886-6-238-9940.
E-mail address: jjmiau@mail.ncku.edu.tw (J.J. Miau).

0889-9746/03/$ - see front matter © 2003 Elsevier Science Ltd. All rights reserved.
doi:10.1016/S0889-9746(03)00007-0

Nomenclature

D	maximum width of the trapezoidal cylinder
f_c	cut-off frequency
I_{Sp}, I_{Mp}, I_{Fp}	the integral time scales of the low-pass spanwise velocity fluctuations measured at Sp, Mp, Fp
Iq_1	integral time scale of a quantity q_1 after being low-pass filtered
P_{ib}	instantaneous base pressure in dimensional unit
P_b	nondimensionalized instantaneous base pressure
$(P_{bL})_{\text{r.m.s.}}$	root-mean-square value of the low-passed P_b signals
$(P_b)_{\text{r.m.s.}}$.	root-mean-square value of the P_b signals
P_r	reference pressure
P_w	pressure fluctuations measured on the wall
q_1, q_2	representation of two instantaneous quantities measured
R	correlation coefficient of the raw signals
Re	Reynolds number, $\text{Re} = DU^*/\nu$
R_L	correlation coefficient of the low-passed signals
St_c	nondimensional cut-off frequency, $\text{St}_c = f_c D/U^*$
Sp, Mp, Fp	three measured locations of the split-fiber probe
t	time
T_c	vortex-shedding period
U_0	free stream velocity
U^*	characteristic velocity, defined as the mean velocity of the flow at the maximum width of the cylinder
U_s	instantaneous streamwise velocity, normalized by U^*
V_L	visibility of low-frequency fluctuations in the base pressure signals measured
X, Y, Z	Cartesian coordinates, shown in Fig. 1a
ΔZ	the spanwise distance between two pressure sensors at the cylinder base
ν	kinematic viscosity of the air
ρ	density of the air
τ	time lag for correlation, normalized by T_c
τ_{R_0}	the time lag corresponding to the first zero crossing in the distribution of R_L versus τ

variations of the vortex-shedding periods read from the trace. Gerrard (1967) reported that the velocity signals obtained in the wakes of circular cylinders at Reynolds numbers between 5000 and 20 000 appeared to contain fluctuations at the vortex-shedding frequency and a less clearly defined frequency an order of magnitude lower. In conducting the velocity measurements in the near-wake region of a circular cylinder at Reynolds numbers of 10 600 and 53 000, Hanson and Richardson (1968) noticed that the velocity fluctuations of long periods, compared to the period of vortex shedding, were prominent in the near-wake region. In addition, a significant amount of experimental and numerical results can be found in the literature concerning various aspects of the phenomenon subjected to different experimental conditions (Schewe, 1983; Blevins, 1985; Williamson, 1992; Szepessy and Bearman, 1992; Yang et al., 1993; Lisoski, 1993; Szepessy, 1994; Blackburn and Melbourne, 1996; Williamson, 1996; Najjar and Balachandar, 1998; Miau et al., 1999).

The low-frequency fluctuations observed in the wake flows were often linked to the three-dimensional characteristics of the vortex-shedding structures (Bloor, 1964; Gerrard, 1966b; Roshko, 1993). The causes leading to the three dimensionality of wake flows can be categorized into the extrinsic and intrinsic effects (Roshko, 1993). Speaking of the extrinsic effect, extensive discussion on the arrangement of end plates and the aspect ratio of a bluff body can be found in the literature. In studying the modulations of the vortex-shedding signal due to the end-plate effect, Gerich and Eckelmann (1982) noticed that the characteristic frequency of beatings in the vortex-shedding signals measured actually corresponded to the difference between the vortex-shedding frequencies measured in the central zone and the affected end zone. They further indicated that beatings could be avoided in the central zone by appropriately manipulating the cylinder end condition. Stäger and Eckelmann (1991) studied the effects of end plate on vortex shedding behind a circular cylinder for Reynolds number in a range of 10^2–10^3. The hot-wire signals were obtained at different spanwise locations from an end plate at $\text{Re} = 130$, which clearly indicated the presence of modulations. As they explained, since the vortex-shedding frequency reduced from the velocity signals measured in the neighborhood of the end plate was different from that measured in the region away from the plate, the interaction of the vortex-shedding frequencies resulted in low-frequency variations.

In studying the effect of the aspect ratio on the two dimensionality of a wake flow, Graham (1969) performed spanwise velocity correlations in the wake behind a D-shaped bluff body with end plates installed. The results obtained showed that the shedding vortices could be regarded as most two dimensional if the aspect ratio was 4 or less. Norberg (1994) showed the effect of aspect ratio of a circular cylinder on the vortex formation length, vortex-shedding frequency and base pressure coefficient at Reynolds numbers of 10^2–10^4. For the aspect ratio at 5 and Reynolds number at 2.7×10^3, low-frequency fluctuations appeared to be significant in the velocity signals measured in the near-wake region. The characteristic frequency associated with the low-frequency unsteadiness reported was estimated to be about 0.015 in the nondimensional value, which was one order of magnitude smaller than the nondimensional vortex-shedding frequency. Norberg (1994) attributed the low-frequency variations measured to the bi-stable flow phenomenon, i.e., a co-existence of the mode of vortex shedding and the irregular mode of no strong periodicity in the wake. Szepessy and Bearman (1992) performed experiments with a circular cylinder of aspect ratios from 0.25 to 12. From the results of fluctuating forces and spanwise correlation of vortex-shedding signals obtained, they concluded that for an aspect ratio of 1, the wake flow appeared to be most two dimensional that the fluctuating lift coefficient measured appeared to be the largest among others, whilst at larger aspect ratios the spanwise incoherence became more pronounced. Fox and West (1990) also showed that the fluctuating lift coefficient of a circular cylinder of aspect ratio 5 was significantly larger than those of aspect ratios at 10, 15 and 25. The effect of end plates on the spanwise uniformity of mean base pressure of a circular cylinder can be learned from the results obtained by Fox and West (1990) and Stansby (1974).

The extrinsic effect can also be due to the structural characteristics of the bluff body. For instance, Gaster (1969) performed measurements in the wake of a tapered cone and clearly showed that low-frequency beatings could be due to the geometrical nonuniformity. Van Atta and Gharib (1987) reported that vibrations of the cylinder due to aero-elastic effects would result in low-frequency unsteadiness in vortex shedding.

Besides the reports in conjunction with the extrinsic effect mentioned above, a brief review on the studies associated with the intrinsic characteristics of the three dimensionality can be given below. Concerning scattering of vortex-shedding frequencies measured in the wake behind a circular cylinder, at Reynolds numbers in the transition range (Roshko, 1954), recent experimental and theoretical evidence suggests that the phenomenon be associated with the development of the three-dimensional instability of the wake flow (Williamson, 1992, 1996; Henderson, 1997). The numerical results of Henderson (1997) showed that at Reynolds number 190 a longer spanwise wavelength corresponding to the onset instability of the so-called mode A, and at Reynolds number 260 a shorter spanwise wavelength corresponding to the onset instability of the so-called mode B could be identified. More interestingly, an earlier work of Hama (1959) presented a photograph at Reynolds number 190 revealing such three-dimensional characteristics of the wake flow. In the paper, a statement was also made concerning the development of the three dimensionality at higher Reynolds numbers. Henderson (1997) showed that modulation in vortex shedding is not perfectly periodic like beating, which is a result of nonlinear interaction between vortex shedding and spanwise oscillations in the separated shear layer. The numerical results of Henderson (1997) at Reynolds number 1000 showed that shedding vortices might develop localized phase dislocations, which were responsible for modulating the amplitude of fluctuating lift and drag. A number of experimental studies (Williamson, 1992, 1996; Yang et al., 1993; Roshko, 1993; Blackburn and Melbourne, 1996) also pointed out the linkage between the dislocation of the spanwise vortex-shedding structures and the presence of low-frequency unsteadiness in the wake flows. On flow over a normal plate, the numerical results of Najjar and Balachandar (1998) showed that the presence of low-frequency unsteadiness in the wake flow is a result of the beating phenomenon due to interaction between the characteristic shedding frequencies in high and low drag regions along the spanwise direction. Also, they pointed out that the formation of shedding vortices was not perfectly synchronized in the spanwise direction, hence the low-frequency unsteadiness could be a result of this imbalance or phase mismatch.

In reality, both of the intrinsic and extrinsic effects mentioned can be present in a wake flow. Lisoski (1993) noticed the presence of low-frequency variations in the force measurements of a cylinder as it is being moved in a quiescent water channel. By increasing the aspect ratio of the cylinder the characteristic period of the low-frequency modulations tended to decrease. However for the aspect ratio larger than 10, the modulation period was maintained fairly constant at about six-fold the vortex-shedding period. As Lisoski (1993) suggested, the results inferred that for an infinite aspect ratio this modulation still exist, which could be due to the instabilities of the wake flow.

In view of the fact that the present experiments were conducted at Reynolds numbers of 10^4, it should be noted that for a wake flow of Reynolds number above 10^3, the separated shear layer originated from the bluff body tends to develop into turbulent motion in the vortex formation region (Roshko, 1954). Hence, in the present wake flow the three-dimensional flow characteristics and the presence of wide-band velocity fluctuations in the near-wake region are expected. Speaking of turbulent shedding vortices, one may refer to a sketch by Kiya and Matsumura (1988) that the vortices are inter-connected by streamwise vortical motions. The flow visualization photographs presented by

Bays-Muchmore and Ahmed (1993) clearly indicated the presence of pair of counter-rotating streamwise vortices immediately downstream of the bluff cylinder, which significantly distorted the vortices shed from the cylinder. Studies of Hanson and Richardson (1968), Szepessy (1994), Miau et al. (1993) and Miau et al. (1999) indicated that for Reynolds numbers in this regime, pronounced low-frequency fluctuations could be detected on the bluff cylinders or in the near-wake regions.

The present work was motivated by the previous concern on the quality of the vortex-shedding signals obtained at a trapezoidal cylinder installed in a circular pipe (Miau et al., 1993). As pointed out in the previous work (Miau et al., 1993), pressure signals measured on a trapezoidal cylinder contained a substantial component of low-frequency variations as the Reynolds numbers were larger than 10^3. Also noted from the energy spectra obtained was that energy associated with the low-frequency variations increased with Reynolds number, where the low-frequency variations referred to those of frequencies lower than the vortex-shedding frequency. Later, Miau et al. (1999) performed experiments with a trapezoidal cylinder of the same cross-sectional shape and a circular cylinder to examine the relation between the low-frequency variations embedded in the base pressure signals measured and the velocity signals measured in the near-wake region. A conclusion obtained in this study was that the low-frequency fluctuations embedded in the vortex-shedding process was closely linked with the unsteady variations of the vortex formation length. Referring to Unal and Rockwell (1988), Bloor and Gerrard (1966), Gerrard (1978) and Blevins (1977) for flows over a circular cylinder, the variations of the time-mean base pressure and the vortex formation length against Reynolds numbers in the range of 10^2–10^5 are well documented. Bearman (1965) showed that the time-mean base pressure varied with the vortex formation length behind a blunt trailing edge, where the base pressure was modified due to a splitter plate of variable length attached downstream. However, the instantaneous relation between base pressure and vortex formation length subjected to a steady incoming flow was rarely reported. Basically, the relation found by Miau et al. (1999) was that the variations of base pressure and vortex formation length with respect to time tended to be out of phase.

The trapezoidal cylinder employed is featured with low aspect ratio and high blockage ratio, shown in Fig. 1a schematically. Referring to Fig. 1a, one realizes that flow separation takes place at the sharp edges of the vortex shedder as far as the present Reynolds numbers are concerned, distinctly different from the situation of flow over a circular cylinder. Further, due to its low aspect ratio and high blockage ratio, caution should be taken if one would like to generalize the present findings to a free flow over a cylinder with high aspect ratio. Nevertheless, the present work was intended to gain further understandings concerning the characteristic behaviors of low-frequency fluctuations previously studied by Miau et al. (1993) and Miau et al. (1999). The methodology described in this paper might be useful for studying other flow configurations in the future.

2. Experimental method

Experiments were performed in a closed-type low-speed wind tunnel, 150 mm × 150 mm in cross-section. Turbulence intensity measured at the center-line of the test section was about 0.7%. Efforts were made to verify that no peculiar fluctuating components were present in the free stream flow and the nonuniformity of the mean flow in the test section, excluding the boundary-layer regions along the walls, was less than $\pm 0.5\%$.

As mentioned, a trapezoidal cylinder was employed as the bluff body, which spanned between two sidewalls of the test section, with the wider side facing the incoming flow, shown in Fig. 1a. Its maximum width was 32 mm, denoted as D. Therefore, the blockage ratio based on the frontal area of the bluff body was about 21%, and the aspect ratio was 4.70.

The Reynolds number, Re, was defined based on D and U^*; U^* denotes the average velocity at the cross-section of the maximum width of the bluff body. Thus, U^* is 1/0.79 times U_0, where U_0 denotes the free stream velocity. During the experiments, the Reynolds numbers were varied in the range of 7.9×10^3–3.24×10^4.

A piezoelectric pressure transducer, PCB103A, 5 mm in diameter, was flush mounted on the rear surface of the cylinder at the mid-span, shown in Fig. 1a, to sense the instantaneous base pressure. According to the specifications provided by the manufacturer, the sensitivity and resolution of the transducer were 0.22 mV/Pa and 0.15 Pa, respectively. The resonant frequency and the lowest frequency response were 13 and 0.05 Hz, respectively. The pressure signals obtained were then nondimensionalized according to the following expression:

$$P_b = \frac{P_{ib} - P_r}{\frac{1}{2}(\rho U^{*2})}, \tag{1}$$

where P_{ib} denotes the instantaneous base pressure measured, P_r denotes a reference pressure measured in the test section, and ρ is the density of air.

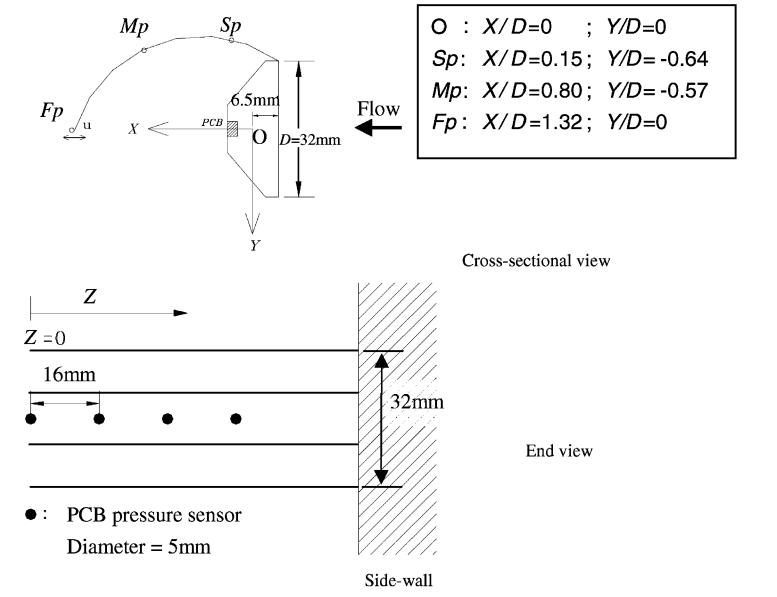

(a) **the trapezoidal cylinder**

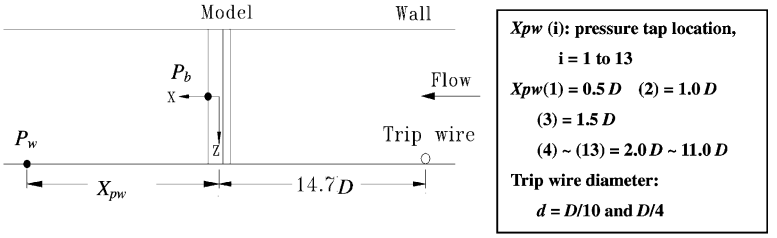

(b) **a schematic view of the test section**

Fig. 1. The experimental arrangement: (a) the trapezoidal cylinder and (b) a schematic view of the test section.

A split-fiber probe, DANTEC 55R55, was employed to acquire the velocity information in the neighborhood of the rear end of the vortex formation region, where the streamwise velocity measured was zero. The probe consists of two parallel nickel-film sensors deposited on a quartz fiber 200 μm in diameter. Calibration of each of the sensors was carried out with the sensor oriented facing the incoming flow. In measuring the streamwise velocity in the near-wake region, the major axis of the split fiber was aligned parallel to the trapezoidal cylinder, such that one of the films was situated on the forward side and the other was situated on the rear side. Hence, by comparing the outputs of the two sensors, one could identify the flow in forward or reversal direction. The streamwise velocity measured by the probe, normalized by U^*, is denoted U_s. The probe could also be employed to sense the unsteady spanwise motions in the separated shear layer originated from the cylinder. In this case, the split fiber was oriented perpendicular to the cylinder, thus the films on the two sides were sensitive to the spanwise velocity component.

The coordinate system employed for the present study is indicated in Fig. 1a. X denotes the streamwise axis pointing downstream, $X = 0$ is located at 6.5 mm downstream of the frontal face of the trapezoidal cylinder. Y and Z denote the vertical and spanwise axes, respectively, that $Y = 0$ and $Z = 0$ is at the center-line of the test section.

To sense the pressure fluctuations on one of the sidewalls of the test section, a piezoelectric pressure sensor, PCB 103A02, was installed beneath the wall surface. The dynamic characteristics of this sensor were verified to be comparable to those of the sensor situated at the mid-span of the cylinder. The pressure measurements were carried out along the center-line of the sidewall at the positions indicated in Fig. 1b. In performing these measurements, the boundary layer on the sidewall could be thickened by a trip wire, 0.1 or 0.25D in diameter, placed 14.7D upstream of the bluff body, as shown schematically in Fig. 1b. The boundary-layer profiles at $X = 0$ with and without the trip wire installed, in the absence of the bluff cylinder, were measured and documented for reference.

3. Data reduction technique

A fifth-order low-pass Butterworth filter was employed to process the signals measured. This filter was characterized by a cut-off frequency, f_c, which was considered a variable in the analysis.

The technique of time-lag correlation was employed to examine the relation between the signal traces measured. The correlation coefficient, $R(q_1, q_2, \tau)$, is defined as follows:

$$R(q_1, q_2, \tau) = \frac{\overline{q_1(t)q_2(t+\tau)}}{\left(\overline{q_1^2}\right)^{1/2}\left(\overline{q_2^2}\right)^{1/2}}. \tag{2}$$

In Eq. (2), q_1 and q_2 represent the instantaneous quantities measured; τ normalized by the characteristic vortex-shedding period, T_c, denotes the time lag between q_1 and q_2. As a counterpart of Eq. (2), $R_L(q_1, q_2, \tau)$ stands for the correlation coefficient of the low-passed traces of q_1 and q_2.

In view of the fact that the low-frequency variations of interest appear irregular in time (Miau et al., 1999), the integral time scale defined in Eq. (3) was employed to describe the low-frequency behavior (Comte-Bellot and Corrsin, 1971).

$$I_{q1} = \int_0^{\tau_{Ro}} R_L(q_1, q_1, \tau)\, \mathrm{d}\tau, \tag{3}$$

where τ_{R_0} denotes the first zero crossing of $R_L(q_1, q_1, \tau)$ on the τ-axis, and $R_L(q_1, q_1, \tau)$ represents the auto-correlation coefficient of the low-passed trace of q_1. $R_L(q_1, q_1, \tau)$ in Eq. (3) is an ensemble-averaged quantity reduced from 10 sets of the correlation coefficient distributions. In determining the size of an ensemble (Bendat and Piersol, 1991), it was checked that the discrepancy between the integral length scales reduced from 10 and 50 distributions was less than 1%.

4. Results and discussion

4.1. General characteristics of low-frequency fluctuations in the near-wake region

Two sets of data concerning the ratio of the integral time scales I_{Us} and I_{Pb} obtained in the near-wake region at Re $=1.65$ and 3.0×10^4, respectively, are shown in Fig. 2. I_{Us} denotes the integral time scale of low-frequency variations embedded in the velocity signals obtained by the split-fiber probe traversing in the region of $X/D = 0.4$ to 10, at $Y = 0$ and $Z = 0$. I_{Pb} denotes the integral time scale of low-frequency variations embedded in the base pressure fluctuations measured simultaneously. The cut-off frequencies of low-pass filtering chosen for Re $= 1.65 \times 10^4$ and 3.0×10^4 were 5.6 and 10.5 Hz, respectively.

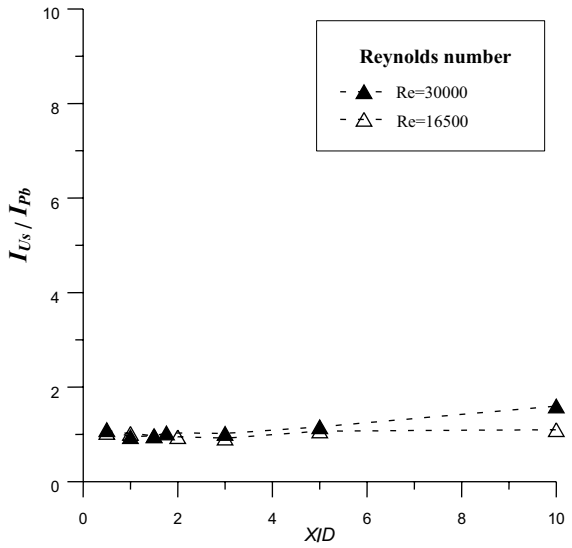

Fig. 2. Variations of (I_{Us}/I_{Pb}) versus the steamwise locations of the split-fiber probe situated.

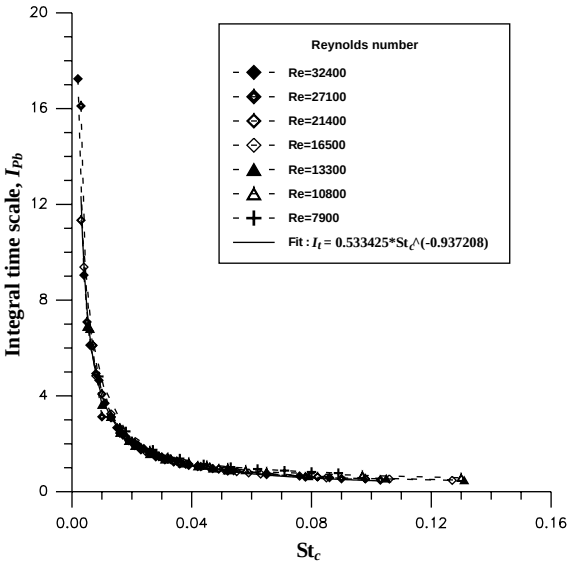

Fig. 3. Integral time scales of the low-passed base pressure fluctuations versus the nondimensional cut-off frequencies (St_c) chosen.

Fig. 2 reveals that for the two cases of Reynolds numbers studied, the integral time scales of I_{Us} and I_{Pb} are almost identical in the vortex formation region, namely, $X/D \leqq 2$. The difference between I_{Us} and I_{Pb} becomes noticeable as the split-fiber probe is moved further downstream. Nevertheless, generally speaking, the low-frequency variations detected at the base of the bluff body and those measured in the near-wake region are of the same time scale. Since measurements by a split fiber require more time and efforts than those by a pressure sensor, in the next section the base pressure data are used for analysis.

4.2. Integral time scale of low-passed base pressure fluctuations versus the nondimensional cut-off frequency

The base pressure measurements were performed at Reynolds numbers between 7.9×10^3 and 3.24×10^4. The reduced integral time scales, normalized by T_c, versus the nondimensional cut-off frequencies

$$\mathrm{St}_c = \frac{f_c D}{U^*} \tag{4}$$

are presented in Fig. 3. Interestingly, the data of different Reynolds numbers studied appear to collapse into a single curve. This curve can be further described by a numerical expression below:

$$I_{pb} = 0.0533\,\mathrm{St}_c^{-0.937}. \tag{5}$$

Note that the numerical curve (5) and the data match so well that the correlation coefficient exceeds 0.99. This curve is of use later to find the integral time scale of low-passed fluctuations with respect to the cut-off frequency chosen. It is also of interest to note that I_{pb} approaches to unity as St_c becomes larger than 0.1. This is attributed to the fact that as the cut-off frequency becomes higher, the fluctuations associated with the vortex-shedding frequency component get in the low-passed trace.

4.3. The optimal cut-off frequency

In this section, correlation between the low-passed traces of P_b and U_s will be examined in reference to different cut-off frequencies chosen. As mentioned, U_s represents the streamwise velocity measured by the split-fiber probe, in the neighborhood of the rear end of the vortex formation region. Subsequently, an optimal cut-off frequency is defined as the one corresponding to the largest negative value of $R_L(P_b, U_s, \tau = 0)$ obtained. This definition was motivated by a concern about how to select a meaningful cut-off frequency since the cut-off frequency was a variable in the present analysis. The optimal cut-off frequency defined corresponds to a situation that the low-passed fluctuations in the base pressure signals and the velocity signals measured are best correlated.

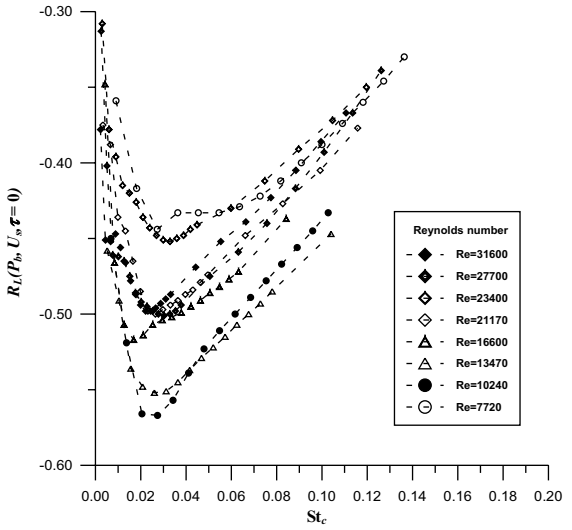

Fig. 4. Distributions of $R_L(P_b, U_s, \tau = 0)$ versus the nondimensional cut-off frequencies, St_c, for Re $=7.72 \times 10^3$–3.16×10^4.

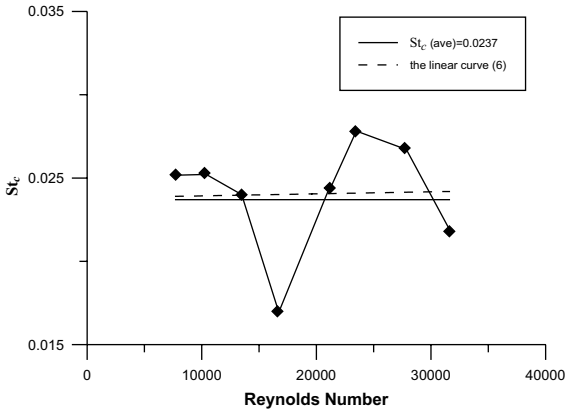

Fig. 5. Optimal cut-off frequencies versus Re between 7.72×10^3 and 3.16×10^4.

Fig. 4 presents the distributions of $R_L(P_b, U_s, \tau = 0)$ versus St_c for Re between 7.72×10^3 and 3.16×10^4. One can identify the optimal cut-off frequency from each of the $R_L(P_b, U_s, \tau = 0)$ distributions shown in the figure. Roughly speaking, the optimal cut-off frequencies seen scatter somewhat with the Reynolds numbers.

Fig. 5 compares the normalized optimal cut-off frequencies obtained at different Reynolds numbers, in which a linear curve depicting the regression of the data shown is also included. The expression of this curve is given below:

$$St_c = 0.000363\,\mathrm{Re} - 0.442. \tag{6}$$

In addition, the average of the optimal cut-off frequencies is also marked in the figure, which is 0.0237. Since the linear curve (6) and the averaged value appear to be quite close, it is fair to say that the optimal cut-off frequencies shown can be represented by the value 0.0237. As noted, the value is about one-sixth of the nondimensional vortex-shedding frequency of the trapezoidal cylinder, which is 0.147. Yang et al. (1993) reported that for flow over a circular cylinder the characteristic frequency of the low-frequency variations observed is about one-sixth of the vortex-shedding frequency. However, it should be pointed out that the experiments of Yang et al. (1993) were conducted at Reynolds numbers in a range of 10^2–10^3, whereas the present Reynolds numbers are in a range of 10^3–10^4. From Fig. 3 or Eq. (5), one can observe that the integral time scale corresponding to $St_c = 0.0237$ is about two times the characteristic vortex-shedding period. This integral time scale is coincidentally equivalent to the characteristic time scale of random shearing stress in the wake behind a normal plate reported by Kiya and Matsumura (1988). However, no further explanation regarding this coincidence can be made here.

4.4. Visibility of low-frequency fluctuations embedded in the base pressure signals

A quantity called the visibility, V_L, is defined here to describe the significance of low-frequency fluctuations embedded in the signals measured

$$V_L = \frac{(P_{bL})_{\text{r.m.s.}}}{(P_b)_{\text{r.m.s.}}}. \tag{7}$$

In Eq. (7), $(P_{bL})_{\text{r.m.s.}}$ denotes the root-mean-square (r.m.s.) value of fluctuations in the low-passed base pressure signal trace; and $(P_b)_{\text{r.m.s.}}$ denotes the r.m.s. value of fluctuations in the raw signal trace measured. Thus, V_L signifies the relative importance of the low-passed fluctuations to the total fluctuations.

Fig. 6 shows the distributions of V_L versus St_c at different Reynolds numbers studied. It is seen in the figure that the V_L values in reference to $\text{St}_c = 0.0237$, that is the optimal cut-off frequency, are about 10%, regardless of the Reynolds numbers studied. In fact, the V_L values appear to be insensitive to the Reynolds numbers for St_c up to 0.3. This is somewhat different from the previous observation that the low-frequency variations became more pronounced with increasing Reynolds number (Miau et al., 1993). Further, the V_L values obtained at $\text{St}_c = 0.147$, which is equivalent to the nondimensional vortex-shedding frequency, appear to be less than 40%, inferring that a substantial portion of the fluctuating energy resides at higher frequencies. This is plausible, because the base pressure fluctuations are mainly induced by alternate vortex shedding, characterized by two times the vortex-shedding frequency. Thus, in the figure, the V_L values appear to increase steeply for St_c up to 0.3. In the neighborhood of $\text{St}_c = 0.3$, equivalent to two times the nondimensional vortex-shedding frequency roughly, the V_L values appear to reach a level of 80%.

4.5. The sidewall effect on the low-frequency variations in vortex shedding

The presence of sidewall was first examined with the correlation between the pressure fluctuations measured on the wall, without a trip wire installed upstream, and the base pressure fluctuations measured at the mid-span of the cylinder. Experiments were carried out at $\text{Re} = 3.2 \times 10^4$. Pressure fluctuations obtained on the sidewall, at $X/D = 2$, and at the mid-span of the cylinder were reduced to the nondimensional quantities, P_w and P_b, respectively. Both of the frequency spectra of P_w and P_b revealed a peak frequency band centered at 135 Hz. This frequency component was identified to be equivalent to two times the vortex-shedding frequency. As mentioned, the pressure fluctuations measured were mainly due to alternate vortex shedding.

In order to examine the characteristics of low-frequency variations in the P_w and P_b signal traces, the raw signals were low-pass filtered at $f_c = 11$ Hz, that is the optimal cut-off frequency determined by Eq. (6). The distribution of $R_L(P_b, P_w, \tau)$ versus τ is shown in Fig. 7a. As seen in the figure, the maximum value of $R_L(P_b, P_w, \tau)$ occurs at $\tau = 0$ and is equal to about 0.3. This appearance reveals the in-phase behavior of low-frequency variations in P_b and P_w,

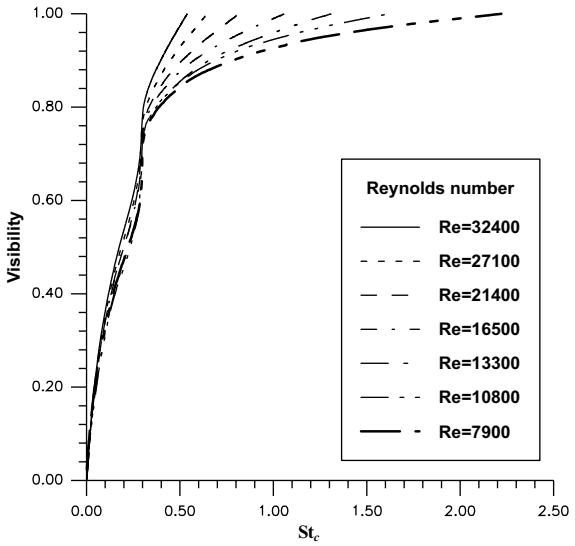

Fig. 6. Variations of V_L versus St_c, the nondimensional cut-off frequency chosen.

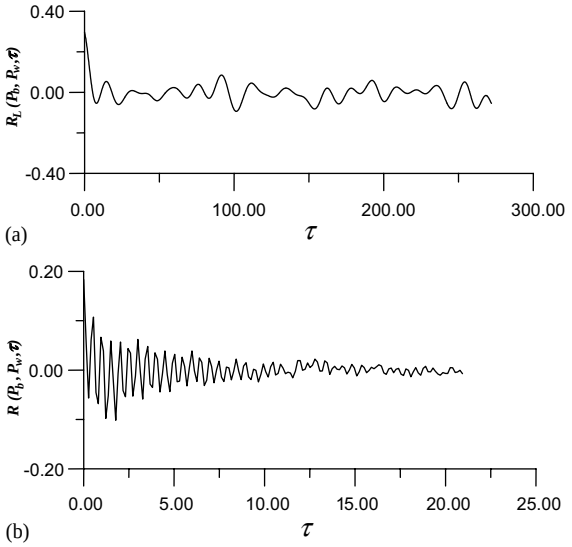

Fig. 7. Distributions of: (a) $R_L(P_b, P_w, \tau)$ and (b) $R(P_b, P_w, \tau)$; P_b and P_w were measured at $X/D = 2$, Re =32 000.

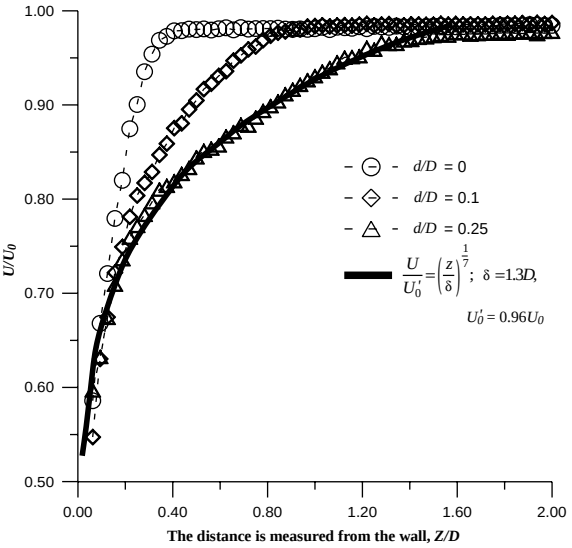

Fig. 8. Velocity profiles measured on the sidewall at $X/D = -0.41$ subjected to three cases of different trip devices situated $14.7D$ upstream of the bluff body.

statistically speaking. It should be mentioned that while the $R_L(P_b, P_w, \tau)$ values at $\tau < 0$ are not shown in the figure, the values are smaller than that of $R_L(P_b, P_w, \tau = 0)$.

As a counterpart of Fig. 7a and b presents the distribution of $R(P_b, P_w, \tau)$ versus τ. The maximum value of $R(P_b, P_w, \tau)$ also occurs at $\tau = 0$ and is about 0.2. As noted, $R(P_b, P_w, \tau = 0)$ is smaller than $R_L(P_b, P_w, \tau = 0)$ in value. In addition, it should be mentioned that $R(P_b, P_w, \tau)$ is mainly due to fluctuations associated with alternate vortex-shedding, hence variations in the $R(P_b, P_w, \tau = 0)$ distribution curve are characterized by one-half of the vortex-shedding period.

The correlation between P_b and P_w was further examined with respect to different sidewall boundary-layer characteristics. As mentioned earlier, the sidewall boundary layer was thickened by a trip wire situated at $X/D = -14.7$. Fig. 8 presents the boundary-layer profiles obtained at $X/D = -0.41$ for the three cases studied, in the absence of the trapezoidal cylinder. For the case without a trip wire situated upstream the boundary-layer thickness is about $0.4D$, whereas for the two cases with the installation of the trip wires of $0.1D$ and $0.25D$ in diameter, the thickness of the

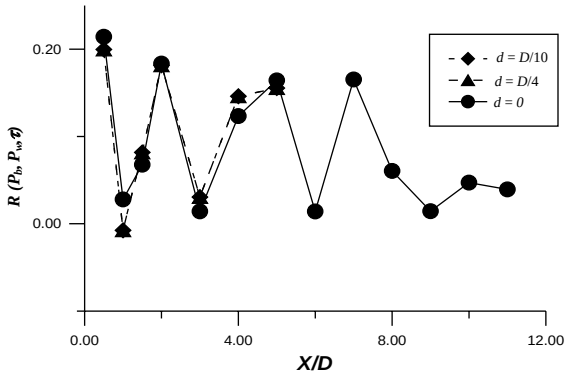

Fig. 9. Correlation coefficients of base pressure signals and pressure signals measured on the sidewall in the region of $X/D = 0$–11, subjected to three cases of different trip devices upstream.

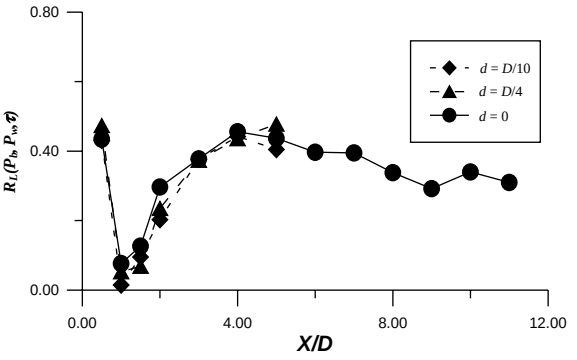

Fig. 10. Correlation coefficients of the low-passed of base pressure and wall pressure signals measured, subjected to three cases of different trip devices upstream.

boundary layers are about $0.8D$ and $1.3D$, respectively. Furthermore, for the latter case, the velocity profile resembles that of a turbulent boundary layer. A curve depicting the one-seventh power law (Schlichting, 1968), which is frequently employed for modeling a flat-plate turbulent boundary-layer profile, is included in the figure for comparison.

The $R(P_b, P_w, \tau = 0)$ values of the three cases studied, with P_w measured in the region of $X/D = 0.5$ to 11, along the center-line of the sidewall, are presented in Fig. 9. In this figure, the horizontal axis indicates the streamwise locations where the measurements of P_w were made. The data of the three cases presented appear to be almost coincided, a strong implication that the correlation between the raw signals of P_b and P_w is insensitive to the alternation of the sidewall boundary-layer characteristics. In the figure, the pronounced variations of the correlation coefficients in the region of $X/D = 2$–9 are likely to be due to the convection of shedding vortices. Since the nondimensional vortex-shedding frequency is 0.147, it can be shown that the streamwise length corresponding to half of the distance between two consecutive shedding vortices is about $3.3D$, which matches roughly with the characteristic scale of the variations seen in the figure in the region of $X/D = 2$–9. Downstream of $X/D = 9$, the correlation coefficients diminishes rapidly. This is attributed to shedding vortices disintegrated into random fluctuations in this region.

As a counterpart of Fig. 10 presents the $R_L(P_b, P_w, \tau = 0)$ values corresponding to the three cases studied, subjected to the optimal cut-off frequency at $f_c = 11$ Hz. Interesting features revealed from a comparison of Figs. 9 and 10 are described below. First, the values of $R_L(P_b, P_w, \tau = 0)$ shown in Fig. 10 are higher than the values of $R(P_b, P_w, \tau = 0)$ in general, except for the measurements of P_w made in the neighborhood of $X/D = 1$. Specifically, the $R_L(P_b, P_w, \tau = 0)$ values corresponding to P_w measured in the region from $X/D = 4$–11 are maintained as high as 0.4, inferring that the coherence of low-frequency variations in the P_b and P_w signals is remarkable. It should be noted that irrespective of the locations of P_w, the results of $R_L(P_b, P_w, \tau)$ obtained always show the maximum value occurred at $\tau = 0$. This implies that the low-frequency variations exhibit an in-phase characteristic in the near-wake region. Secondly, the sharp decrease of $R_L(P_b, P_w, \tau = 0)$ taking place in the neighborhood of $X/D = 1$ is speculated to be due to the presence of horse-shoe vortices at the junction of the bluff body and the sidewall. However, no further efforts were made to verify

this speculation. Thirdly, similar to Fig. 9, the data of the three cases shown in Fig. 10 tend to collapse together, inferring that varying the sidewall boundary-layer characteristics exerts little effect on low-frequency variations in vortex shedding.

Based on the features of Figs. 9 and 10 mentioned above, two statements can be further made below. First, the sidewall boundary layer does not play an active role to affect the development of low-frequency variations in vortex shedding, because little differences were noted among the three cases presented in Figs. 9 and 10. Second, the signature of low-frequency variations in vortex shedding can be clearly detected on the sidewall at least up to $10D$ downstream of the bluff body, hence the low-frequency variations of interest are well noticeable in the near-wake region.

4.6. The linkage between low-frequency variations and three dimensionality of the wake flow

The three-dimensional flow characteristics in the near-wake region were examined with the correlation of base pressure signals obtained at different spanwise locations. Table 1(a) lists the results of cross-correlation at $\tau = 0$. for two pressure sensors situated at the rear face of the cylinder, separated by $\Delta Z/D = 0.5$, 1 and 1.5, respectively. Note that for each of the cross-correlation, the correlation coefficient at $\tau = 0$ is the largest compared to those obtained at $\tau \neq 0$ Experiments were conducted with the reference sensor fixed at the mid-span of the cylinder, $Z = 0$, while the other could be situated at $Z/D = 0.5$, 1 or 1.5. One may refer to Fig. 1a for the spanwise locations of pressure measurement schematically. The experiment was carried out at $\mathrm{Re} = 1.63 \times 10^4$.

Features obtained from Table 1(a) can be summarized as follows. First, all the correlation coefficients shown in the table, irrespective of raw signals or low-pass filtered traces, are less than 0.4, indicating that the three dimensionality of the wake flow is pronounced. Note that the cut-off frequency chosen, $f_c = 5.5$ Hz, was the optimal cut-off frequency determined according to Eq. (6). Second, the correlation coefficients of low-passed traces appear to be higher in value compared to those of the raw signals. This appearance implies that spanwise coherence of low-frequency variations is superior to that of raw signals, which were dominated by the fluctuating components at vortex-shedding frequency and its harmonics. Third, the correlation coefficients of low-passed signals are maintained fairly constant with respect to the spanwise separations of $\Delta Z/D = 0.5$, 1 and 1.5, inferring that the spanwise length scale associated with the low-frequency variations of interest can be significantly beyond $1.5D$.

Similar to Table 1(a) and (b) presents the spanwise correlation coefficients obtained at $\mathrm{Re} = 2.56 \times 10^4$. Again, the cut-off frequency chosen, $f_c = 8.9$ Hz, was the optimal cut-off frequency determined by Eq. (6). This table basically shows the same features as those noted in Table 1(a). The correlation coefficient of the low-passed traces at $\Delta Z/D = 1.5$ decreases to 0.23, lower than that seen in Table 1(a). This seems to infer that the correlation might get less significant as Reynolds number increases.

Three dimensionality of the wake flow was further studied by examining the spanwise motions of separated shear layer in the near-wake region. This was carried out using a split-fiber probe placed in the separated shear layer. As mentioned earlier, the fiber probe oriented in the Y direction, hence the thermal films on the two sides of the probe were sensitive to the spanwise velocity component. By comparing the outputs of the two thermal films, one could tell the direction of the instantaneous spanwise velocity.

The split-fiber probe was placed at three locations in the shear layer, denoted as *Sp*, *Mp* and *Fp*, indicated in Fig. 1a schematically. *Sp*, *Mp* and *Fp* were at $(X/D, Y/D, Z/D) = (0.15, -0.64, 0)$, $(0.80, -0.57, 0)$ and $(1.32, 0, 0)$, respectively.

Table 1
Cross-correlation coefficients at time-lag $\tau = 0$ for base pressure fluctuations obtained with $\Delta Z/D = 0.5$, 1 and 1.5 at (a) $\mathrm{Re} = 16\,300$ and (b) $\mathrm{Re} = 25\,660$

$\Delta Z/D$	$R_L(\Delta Z, \tau = 0)$	$R(\Delta Z, \tau = 0)$
(a)		
0.5	0.38	0.32
1	0.35	0.30
1.5	0.34	0.18
(b)		
0.5	0.34	0.31
1	0.34	0.21
1.5	0.23	0.16

Table 2
Integral time scales of low-frequency variations sensed by the split fiber at the locations of *Sp*, *Mp* and *Fp*

	$Re = 1.6 \times 10^4$	$Re = 2.55 \times 10^4$	$Re = 3.12 \times 10^4$
f_c (Hz)	5.6	8.6	10.5
I_{Sp}	1.8	1.8	1.8
I_{Mp}	1.6	1.7	1.7
I_{Fp}	1.6	1.7	1.6

Namely, *Sp* was located near the sharp edge of the cylinder, *Mp* was located between *Sp* and *Fp*, and *Fp* was located close to the rear end of the vortex formation region.

Table 2 shows the normalized integral time scales of the low-passed signals obtained at the locations of *Sp*, *Mp* and *Fp*, denoted as I_{Sp}, I_{Mp}, and I_{Fp}, respectively, at Re $=1.66 \times 10^4$, 2.55×10^4 and 3.12×10^4. Note that the raw signals were obtained from one of the two thermal films on the split-fiber probe. The cut-off frequencies shown in the table were the optimal cut-off frequencies determined by Eq. (6). As revealed from the table, the I_{Sp}, I_{Mp}, and I_{Fp} values appear to vary in a range between 1.6 and 1.8. Coincidentally, it is noted from Fig. 3 that $I_{pb} = 2$ is the integral time scale of the low-passed base-pressure fluctuations subjected to the same cut-off frequency. Hence, the closeness between the $I_{Sp}, I_{Mp} I_{Fp}$ and I_{pb} values seems to suggest that the unsteady, spanwise motions of the separated shear layer be associated with the low-frequency variations seen in the vortex-shedding process.

Humphreys (1960) reported experimental observations concerning spanwise motions in separated shear layers from a bluff body, which were revealed by threads attached to the bluff body. Humphreys (1960) addressed that the threads not only flapped with the wake flow, but also showed some spanwise irregularity at low Reynolds number. When the speed was raised to the Reynolds number of 10^5, remarkable unsteady motions of the threads were observed. He further pointed out that large-scale random fluctuations seen in the lift and drag measurements could be tied to wake modulation, featured by the three-dimensional motion.

Based on the experimental results presented above, a physical picture regarding the low-frequency variations in vortex shedding and the three dimensionality of the wake flow can be proposed below. Given the fact that the three dimensionality is intrinsic in the separated shear layer at Reynolds number above 10^3, the low-frequency variations seen in the vortex-shedding process are considered to be associated with the global change of three-dimensional flow pattern in the near-wake region with time. By the three-dimensional flow pattern, it means that the separated shear layer is featured with a spanwise velocity component varying with space and time. Accordingly, the vortex formation length might not be uniform in the spanwise direction, and shedding vortices might not align perfectly along the spanwise axis even at the initial stage of shedding. The global change of the three-dimensional flow pattern implies that the three-dimensional flow pattern described above could alter over the entire near-wake region instantaneously, although the mechanism is not clear at present. One of the possibilities could be due to the mechanism of absolute wake instability described by Huerre and Monkewitz (1990). The global characteristics of low-frequency variations can be realized from the results of Figs. 7a and 10 as well. Another finding is that the cross-correlation of low-passed base pressure fluctuations and sidewall pressure fluctuations is maximum at zero time-lag, regardless of the streamwise locations of sidewall pressure measured. Further evidence can also be found in the previous study (Miau et al., 1999) that correlation between low-passed velocity fluctuations obtained at the rear end of the vortex formation region and low-passed base pressure fluctuations gave the most negative value at zero time lag.

5. Concluding remarks

In this study, a quantitative analysis was performed to study the characteristic behaviors of low-frequency variations embedded in vortex shedding. The experimental data obtained at Reynolds numbers in a range from 7.9×10^3–3.24×10^4 were analyzed. Major findings can be summarized as follows:

(i) The characteristic behaviors of the low-frequency variations, in terms of the nondimensional quantities defined, are found to be insensitive to the Reynolds numbers studied.
(ii) Variations of the integral time scales associated with the low-passed base pressure fluctuations versus the cut-off frequencies chosen fall on a curve, irrespective of the Reynolds numbers studied.
(iii) The optimal cut-off frequencies found in the present study can be represented by a nondimensional value, 0.0237, which is about one-sixth of the nondimensional vortex-shedding frequency, 0.147.

(iv) The integral time scale of low-passed base-pressure signals in reference to the optimal cut-off frequency is about two times the characteristic period of vortex shedding.
(v) The ratio of the r.m.s. intensity of low-passed base pressure fluctuations in reference to the optimal cut-off frequency versus that of the total fluctuations is about 10%. This quantifies the significance of low-frequency fluctuations in the vortex-shedding process.
(vi) The low-frequency fluctuations observed in the near-wake region exhibit a global characteristic, which could be linked to the spanwise motions in the separated shear layer.

Acknowledgements

This work was supported by National Science Council, Republic of China, under the contract number NSC 85-2622-E-006-018. The authors would also like to thank Mr. S.J. Wu for his help on wind tunnel calibration.

References

Bays-Muchmore, B., Ahmed, A., 1993. On streamwise vortices in turbulent wakes of cylinders. Physics of Fluids 5, 387–392.
Bearman, P.W., 1965. Investigation of the flow behind a two-dimensional model with a blunt trailing edge and fitted with splitter plates. Journal of Fluid Mechanics 21, 241–255.
Bendat, J.S., Piersol, A.G., 1991. Random Data Analysis and Measurement Procedures, 2nd Edition. Wiley, New York.
Blackburn, H.M., Melbourn, W.H., 1996. The effect of free-stream turbulence on sectional lift forces on a circular cylinder. Journal of Fluid Mechanics 306, 267–292.
Blevins, R.D., 1977. Flow-Induced Vibration. Van Nostrand Reinhold, New York.
Blevins, R.D., 1985. The effect of sound on vortex shedding from cylinders. Journal of Fluid Mechanics 161, 217–237.
Bloor, M.S., 1964. The transition to turbulence in the wake of a circular cylinder. Journal of Fluid Mechanics 19, 290–304.
Bloor, M.S., Gerrard, J.H., 1966. Measurements on turbulent vortices in a cylinder wake. Proceedings of the Royal Society of London A 294, 319–342.
Comte-Bellot, G., Corrsin, S., 1971. Simple Eulerian time correlation of full- and narrow-band velocity signals in grid-generated isotropic turbulence. Journal of Fluid Mechanics 48, 273–337.
Fox, T.A., West, G.S., 1990. On the use of end plates with circular cylinders. Experiments in Fluids 9, 237–239.
Gaster, M., 1969. Vortex shedding from slender cones at low Reynolds numbers. Journal of Fluid Mechanics 38, 565–576.
Gerich, D., Eckelmann, H., 1982. Influence of end plates and free ends on the shedding frequency of circular cylinders. Journal of Fluid Mechanics 122, 109–121.
Gerrard, J.H., 1966a. The three-dimensional structure of the wake of a circular cylinder. Journal of Fluid Mechanics 25, 143–164.
Gerrard, J.H., 1966b. The mechanics of the formation region of vortices behind bluff bodies. Journal of Fluid Mechanics 25, 401–413.
Gerrard, J.H., 1967. Experimental investigation of separated boundary layer undergoing transition to turbulence. Physics of Fluids 10, S98–100.
Gerrard, J.H., 1978. The wakes of cylindrical bluff body at low Reynolds number. Philosophical Transactions of the Royal Society of London A 288, 351–382.
Graham, J.M.R., 1969. The effect of end-plates on two-dimensionality of a vortex wake. The Aeronautical Quarterly 20, 237–247.
Hama, F.R., 1959. Three-dimensional vortex pattern behind a circular cylinder. Journal of the Aeronautical Sciences 24, 156–158.
Hanson, F.B., Richardson, P.D., 1968. The near-wake of a circular cylinder in crossflow. Journal of Basic Engineering, Transactions of ASME 90, 476–484.
Henderson, R.C., 1997. Nonlinear dynamics and pattern formation in turbulent wake transition. Journal of Fluid Mechanics 352, 65–112.
Huerre, P., Monkewitz, P.A., 1990. Local and global instabilities in spatially developing flows. Annual Review of Fluid Mechanics 22, 473–537.
Humphreys, J.S., 1960. On a circular cylinder in a steady wind at transition reynolds numbers. Journal of Fluid Mechanics 9, 603–612.
Kiya, M., Matsumura, M., 1988. Incoherent turbulent structure in the near wake of a normal plate. Journal of Fluid Mechanics 190, 343–356.
Lisoski, D., 1993. Nominally 2-dimensional flow about a normal flat plate. Ph.D. Thesis, California Institute of Technology.
Miau, J.J., Yang, C.C., Chou, J.H., Lee, K.R., 1993. Suppression of low-frequency variations in vortex shedding by a splitter plate behind a bluff body. Journal of Fluids and Structures 7, 897–912.
Miau, J.J., Wang, J.T., Chou, J.H., Wei, C.Y., 1999. Characteristics of low-frequency variations embedded in vortex shedding process. Journal of Fluids and Structures 13, 339–359.
Najjar, F.M., Balachandar, S., 1998. Low-frequency unsteadiness in the wake of a normal flat plate. Journal of Fluid Mechanics 370, 101–147.

Norberg, C., 1994. An experimental investigation of the flow around a circular cylinder: influence of aspect ratio. Journal of Fluid Mechanics 258, 287–316.

Roshko, A., 1954. On the development of turbulent wakes from vortex streets. NACA Report 1191.

Roshko, A., 1993. Perspectives on bluff body aerodynamics. Journal of Wind Engineering and Industrial Aerodynamics 49, 79–100.

Schewe, G., 1983. On the force fluctuations action on a circular cylinder in crossflow from subcritical up to transcritical Reynolds numbers. Journal of Fluid Mechanics 133, 265–285.

Schlichting, H., 1968. Boundary-Layer Theory (Translated by J. Kestin). McGraw-Hill Book Company, New York (Chapter 21).

Stäger, R., Eckelmann, H., 1991. The effect of endplates on the shedding frequency of a circular cylinders in the irregular range. Physics of Fluids 3, 2116–2121.

Stansby, P.K., 1974. The effects of end plates on the base pressure coefficients of a circular cylinder. Aeronautical Journal 78, 36–37.

Szepessy, S., 1994. On the spanwise correlation of vortex shedding from a circular cylinder at high subcritical Reynolds number. Physics of Fluids 6, 2406–2416.

Szepessy, S., Bearman, P.W., 1992. Aspect ratio and end plate effects on vortex shedding from a circular cylinder. Journal of Fluid Mechanics 234, 191–217.

Tritton, D.J., 1959. Experiments on the flow past a circular cylinder at low Reynolds number. Journal of Fluid Mechanics 16, 547–567.

Unal, M.F., Rockwell, D., 1988. On vortex formation from a cylinder Part 1. The initial instability. Journal of Fluid Mechanics 190, 491–512.

Van Atta, C.W., Gharib, M., 1987. Ordered and chaotic vortex streets behind circular cylinders at low Reynolds numbers. Journal of Fluid Mechanics 174, 113–133.

Williamson, C.H.K., 1992. The natural and forced formation of spot-like vortex dislocations in the transition of a wake. Journal of Fluid Mechanics 243, 393–441.

Williamson, C.H.K., 1996. Vortex dynamics in the cylinder wake. Annual Review of Fluid Mechanics 28, 477–539.

Yang, P.M., Hussein, M., Williams, D.R., 1993. Oblique and parallel wave interaction in the near wake of a circular cylinder. Physics of Fluids 5, 1657–1661.